Petroleum Science 23 (2026) 4939–4950

Contents lists available at ScienceDirect

Petroleum Science

journal homepage: www.keaipublishing.com/en/journals/petroleum-science

Original Paper

Defining conductivity optimal correlation resolution (COCR) for 3D scanning of acid fracture surface

Yi-Fan Dai [a,b,*], Bing Hou [a,b], Zhen-Yu Wang [c,d], Lin-Jun Zou [e], Ming-Fang He [e], Shi-Hui Gao [e]

[a] *Department of Petroleum Engineering, China University of Petroleum (Beijing) at Karamay, Karamay, 834000, Xinjiang, China*
[b] *Xinjiang Key Laboratory of Carbon Efficient Utilization and Storage, China University of Petroleum (Beijing) at Karamay, Karamay, 834000, Xinjiang, China*
[c] *ZhenHua Oil Company, Beijing, 100032, China*
[d] *Chengdu North Petroleum Exploration and Development Technology Company Limited, Chengdu, 610213, Sichuan, China*
[e] *Oil and Gas Technology Research Institute of PetroChina Changqing Oilfield Company, Xi'an, 710016, Shaanxi, China*

A R T I C L E I N F O

Article history:
Received 1 September 2025
Received in revised form
3 January 2026
Accepted 21 April 2026
Available online 30 April 2026

Edited by Meng-Jiao Zhou

Keywords:
Acid fracturing
Fracture conductivity
3-D scanning
Conductivity optimal correlation resolution
Correlation analysis

A B S T R A C T

Production from carbonate reservoirs can be significantly improved through acid fracturing. Creating acid fractures with high conductivity is a key factor in enhancing production. 3D scanning technology enables the digital study of fracture conductivity. It is unclear that how to select the suitable resolution during 3D scanning. This study aims to obtain the conductivity optimal correlation resolution (COCR) for acid fracture research. The 3D scanning result obtained at COCR exhibits the optimal correlation with the fracture conductivity. Experiments involving 3D scanning, fracture conductivity tests, and roughness evaluations were conducted in this research. The experimental results showed that: (1) Acid etching would enhance fracture roughness and conductivity. The strength of the fracture surface would decrease with acid etching, which leads to the significant decreasing of the fracture conductivity under high closure pressure. (2) The roughness evaluation based on Gaussian curvature demonstrated advantages, which can evaluate the roughness from a local view and build a global evaluation method with the fracture conductivity. (3) In acid fracture research, scanning at the resolution of 0.1 mm maximized the roughness-conductivity correlation, which can be defined as COCR. These conclusions provide a reference for selecting 3D scanning resolution in digital studies of acid fracture conductivity.

1. Introduction

Tight carbonate reservoirs contain abundant oil and gas resources due to their substantial storage capacity (Rashid et al., 2015; Qi et al., 2020; Al-Anazi et al., 1998). However, these reservoirs are characterized by low permeability and porosity, which lead to the challenges for efficient development. Acid fracturing, as an advanced stimulation technology, has been widely used in tight carbonate reservoirs (Aljawad et al., 2020; Li et al., 2024; Lai et al., 2022). Acid fracturing fluid would be injected into the wellbore to obtain high pressure and form artificial fractures. Simultaneously, the acid fluid enters these fractures and reacts with carbonate components in the rock, etching the fracture surfaces and generating roughness (Zhou et al., 2021). Several studies (Gou et al., 2023; Feng et al., 2021) have demonstrated that the rough acid-etched fracture surface does not close completely after this process, which can significantly improve the drainage radius and flow capacity near-wellbore region. Consequently, the roughness of acid fracture surfaces and their production-enhancing effects have become hot topics, attracting significant attention from investigators.

Fracture conductivity is a parameter that quantitatively describe the fracture's capacity to transmit fluids under specific closure pressure (Zhong et al., 2019). Relevant studies (Asadollahpour et al., 2018; Zimmerman and Bodvarsson, 1996) have demonstrated that the rough surface would lead to the high fracture conductivity. In acid fracturing, achieving rough fracture surface and high

* Corresponding author.
E-mail address: daiyifan@cupk.edu.cn (Y.-F. Dai).
Peer review under the responsibility of China University of Petroleum (Beijing).

https://doi.org/10.1016/j.petsci.2026.04.038
1995-8226/

conductivity is one of the engineering goals (Malagon et al., 2008; Williams and Nierode, 1972). Engineers hope to obtain the high and stable fracture conductivity to increase oil and gas production. In order to get the best acid fracturing result, theoretical analysis, numerical simulation, and laboratory experiments need to be done in the early stage (Wei et al., 2021; Li et al., 2022). Theoretical analysis always needs idealized assumptions during model formulation, which made it hard to work in multifaceted field conditions (Xue et al., 2020; Guo et al., 2017). Numerical simulation, while serving as practical supplements for fracture characterization, exhibits constrained precision when coupling stress evolution, multiphase flow dynamics, and chemo-mechanical interactions (Sun et al., 2019; Yang and Wen, 2017). Now, the test of the fracture conductivity relies on the laboratory experiments (Hou et al., 2017). For example, in American Petroleum Institute (API) fracture conductivity testing, the fractured sample is subjected to confining pressures and temperatures within a conductivity cell. The difference between the inlet and outlet pressures and the size of the fractured sample can be used to get conductivity curves. Most rock samples are damaged after these experiments. Therefore, while laboratory experiments provide reliable data, they are limited by low repeatability.

With the development of engineering technology, the acid fracturing has become increasingly complex. Temporary plugging acid fracturing (TPAF) (Wang et al., 2020, 2021; Zhou et al., 2022) can selectively seal high-permeability zones to redirect acid flow toward underutilized fractures, thereby enhancing reservoir stimulation efficiency. Meanwhile, injecting proppants after acid fracturing has gradually become a new type of engineering technology (Bale et al., 2010; Zhang et al., 2018). These novel methods have increased the complexity of acid fracture conductivity research, creating a higher demand for laboratory experiments. In recent years, some researchers (Chen et al., 2015) proposed a fracture-surface reconstruct technology based on 3D scanning. This technology can address the issue of poor experimental repeatability by utilizing 3D scanning data and 3D printing. By creating several same fracture surfaces boards, the researchers can optimize construction scheme, like temporary plugging agent or proppant agent, by conducting repeated fracture conductivity experiments with the same acid fracture surface. It is more exciting that the 3D-scanning results can serve as the geometric basis of numerical simulation (Li et al., 2021). These researches have made 3D scanning a promising method. The critical role of accurate fracture characterization for predicting reservoir performance has been further highlighted in recent studies (Liu et al., 2024; Wu et al., 2025).

There are various methods for evaluating the roughness of the fracture surface (Lange et al., 1993; Arakawa and Takahashi, 1991), including the arithmetic mean roughness (Ra), root mean square roughness (Rq), and maximum peak-to-valley height (Rz) and other. The joint roughness coefficient (JRC), which has been a well-established and widely recognized standard in rock mechanics for quantifying macroscopic roughness (Li and Zhang, 2015; Tse and Cruden, 1979), was originally developed for natural joint roughness and shear strength estimation. It has been widely used for roughness quantification due to its simple form and easy estimation. The Gaussian curvature based on laser scanning can also be used to evaluate the roughness of the soil surface, which is also a hot technology (Prajapati and Tiwari, 2017). However, the evaluated roughness has scale effect at different resolutions, which leads to difficulties in 3D-scanning. The researchers need to get 3D coordinates of fracture surface by advanced camera. The resolution is determined by the distance between the 3D coordinates, which is a key evaluation indexes of 3D scanning. Tatone and Grasselli (2013) proved that the roughness values change with the resolution. That means the reconstructed acid fracture surfaces under different resolutions might lead to different experiment results, which would bring uncertainty to the subsequent research.

Current researchers (Brasington et al., 2012; Mendez-Vilas et al., 2007; Kerckhofs et al., 2013) often recommend using the highest resolution to scan. It is hard to accurately answer that at what specific resolution the study of acid fracture surface has sufficient repeatability and the experiment results can adopt. In this paper, we attempt to define the conductivity optimal correlation resolution (COCR for short), which is a specific resolution scale for 3D scanning. The roughness evaluated at that resolution has the best correlation with the acid-etched fracture conductivity. This study aims to find the COCR by analyzing the relationship between the 3D-scanning results and the acid-etched fracture conductivity. The acid fracture surfaces were scanned with different resolutions. The Gaussian curvature and joint roughness coefficient were used to evaluate the roughness. By studying the correlation between roughness and conductivity, the resolution which has the strongest correlation with conductivity was found. We believe that this research achievement can provide a reference standard for 3D-scanning and 3D-printing for the subsequent experimental study of acid fractures.

Our paper mainly consists of the following parts: In Section 2, the conductivity test, 3D scanning technology and experimental schemes are introduced. In Section 3, the experimental results are shown and the COCR are estimated. In Section 4, the applicable conditions of research results and the future research directions are discussed.

2. Experimental methodology

2.1. Experimental sample and acid fracture etching scheme

In acid fracturing, the acid-rock reaction in heterogeneous rocks would lead to random wormholes acid-etched channels (Dai et al., 2021; Hou et al., 2021). The target of study is to establish a methodological benchmark for 3D scanning. The local randomness in acid fracture would introduce interfering factors to the experiments. The rock sample used in our experiments was from the Qixia Group in the Sichuan Basin. The carbonate rocks had the characteristics of high dense degree, high homogeneity and great strength. There were few natural fractures and holes in the rock samples, and the uniformity is relatively good. This provided a controlled and reproducible foundation for clearly and accurately defining of COCR. The specific physical parameters are shown in Table 1.

In this study, the gelled acid, a common acid fracturing fluid in oil fields, was chosen as experimental fluid. The acid formulation was 10% hydrochloric acid +1% acid thickener +2.5% inhibitor main agent +0.5% inhibitor synergist +1.0% iron-ion stabilizer +1.0% cross-linking agent. The equation for rock-acid reaction is:

$$CaCO_3 + 2HCl = CaCl_2 + H_2O + CO_2 \quad (1)$$

The real acid fracture surfaces are generated by rock mass breaking and acid etching. These two processes bring randomness to the acid fracture shape and roughness. To reduce the

Table 1
Physical properties of tight carbonate rocks.

Property	HDR reservoir
Young's modulus, GPa	35.00
Poisson's ratio	0.20
Rock density, kg/m^3	2680.00

uncertainty in our research, wire cutting was used to obtain the same and smooth fracture surfaces initially. Then the gelled-acid would be used to etch the fracture surface. Specifically, the acid fluid would pass through the fracture surface with the constant flow rate under different time, which leads to acid fracture surfaces with controllable differences. The overall preparation workflow is illustrated in Fig. 1.

In our research, all rock samples were cut into standard-sized plates (length: 177.00 mm, width: 38.0 mm). After different times of acid etching, fracture surfaces with different roughness were obtained. The scheme was shown in Table 2.

All rock samples came from the homogeneous carbonate block and stable wire cutting, which means the initial surface conditions were reproducible across all samples. Sample 1# was not etched and designated as the control sample. The subsequent samples (2# to 6#) were the experimental groups. Different fracture surfaces were obtained by subjecting the rock samples to acid etching for different times.

Table 2
Acid fracture etching scheme.

No.	Type of the rock	Acid etching time, min
1#	Carbonate rock	0
2#	Carbonate rock	5
3#	Carbonate rock	10
4#	Carbonate rock	15
5#	Carbonate rock	20
6#	Carbonate rock	25

2.2. Acid fracture conductivity test

After acid etching, the strength of the rock would decrease. When the closed pressure loading time is long enough, slow deformation would occur on the acid fracture surface, changing the roughness and conductivity. During the long-term fracture conductivity experiment, it is unable to precisely measure the deformation degree and get specific morphology of the fracture surface. Considering the simplicity of data analysis, short-term fracture conductivity experiments were chosen and conducted in our research.

The fracture conductivity equipment was shown in Fig. 2, which can test fracture conductivity under different closure pressures. During the experiment, the rock plate would be loaded into the diversion chamber, and a certain closing stress was applied. The fluid was driven into the fracture at a constant flow rate. The pressure difference between the inlet side and the outlet side was measured and the conductivity was calculated after the outlet flow rate was stable.

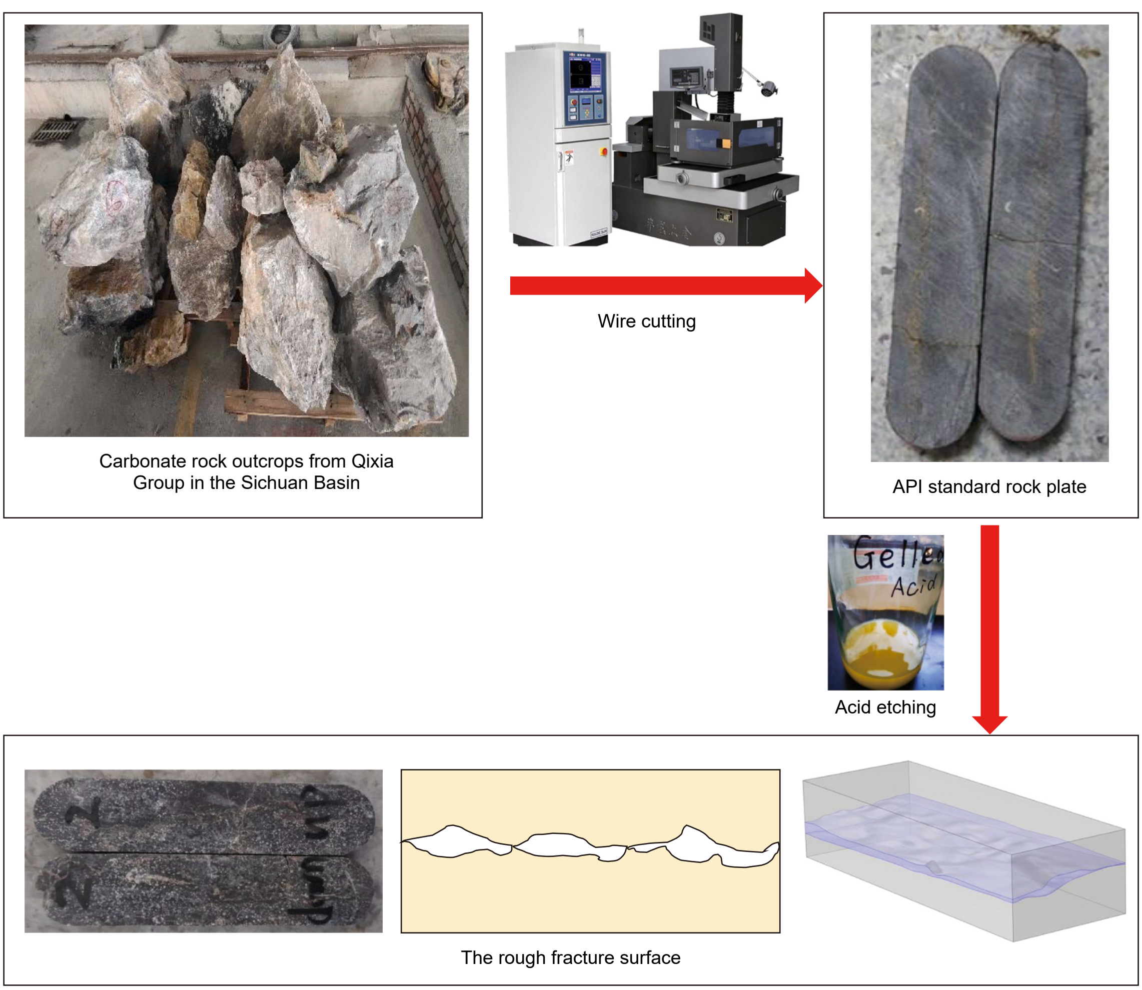

Fig. 1. Flowchart of the preparation process of acid-etched fracture samples.

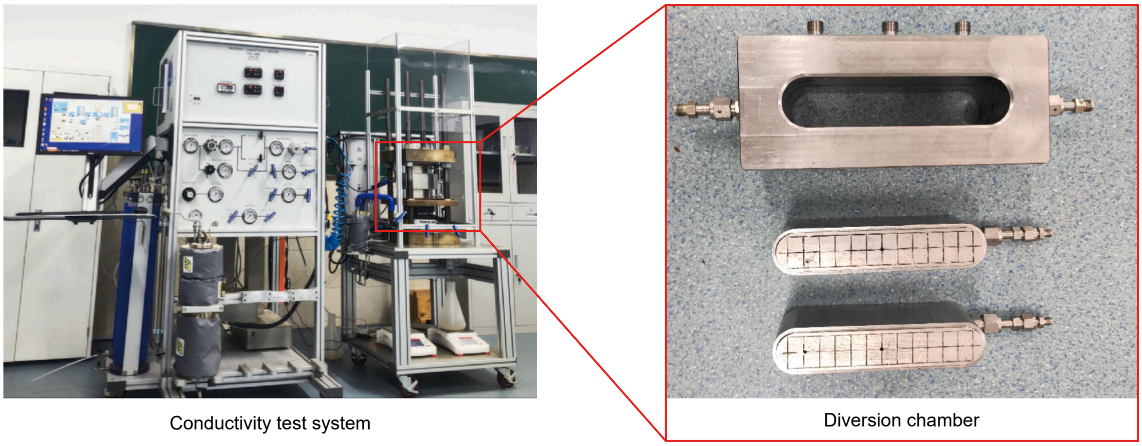

Fig. 2. Acid fracture conductivity test system that complies with API standards.

The effect of time is not considered in this experiment and only the short-term conductivity would be calculated (Sun et al., 2019; Andrews, 2020; Wei et al., 2021). The fracture conductivity can be calculated as:

$$\zeta = \frac{\mu \cdot Q \cdot L}{A \cdot \Delta p} \cdot W_f \tag{2}$$

Here, ζ is the fracture conductivity, mD·cm; μ is the fluid viscosity, mPa·s; Q is the fluid flow rate, m^3/s; L is the fracture length, m; A is the fracture area, m^2; Δp is the pressure difference, Pa; W_f is the fracture width, m.

2.3. 3D-scanning experiment

The 3D-scanning equipment was shown in Fig. 3. Based on the principle of optical triangulation, a series of coding gratings are projected onto the object surface by the projection module, and the corresponding modulated image is obtained by the acquisition module. Then, the coordinate position of 3D point cloud data would be obtained.

This technology does not directly contact with the measured object, but uses visible light that interacts with the object surface. It will not destroy the acid fracture morphology and is convenient to protect the core. As shown in Fig. 4, the fracture surface was scanned and 3D coordinates were extracted. Different scanning resolutions result in different distances between 3D points.

In this study, we conducted batch scans of the fracture surfaces using the following levels of resolution rates, including 0.05 mm, 0.1 mm, 0.2 mm and 0.4 mm.

2.4. Roughness evaluation

The influence of resolution on the correlation between roughness and conductivity was the research focus. In this study, two roughness evaluation methods were adopted to evaluate the surface roughness. The joint roughness coefficient (JRC) was selected to evaluate the overall roughness and the absolute value of Gaussian curvature was selected to evaluate the local roughness. The joint roughness coefficient is a critical parameter in rock mechanics and geotechnical engineering, which can be used to quantify the surface roughness. It provides a benchmark for comparing the roughness-conductivity relationship observed in this study with prior art. The tilt test (Fig. 5) was used to obtain JRC.

The calculation formula of JRC is as follows:

$$\mathrm{JRC} = \frac{\alpha_{\mathrm{Dip}} - \phi_{\mathrm{R}}}{\log_{10}\left(\frac{\mathrm{JCS}}{\sigma_n}\right)} \tag{3}$$

Here, α_{Dip} is the rock-dipping angle,°; ϕ_{R} is the residual friction

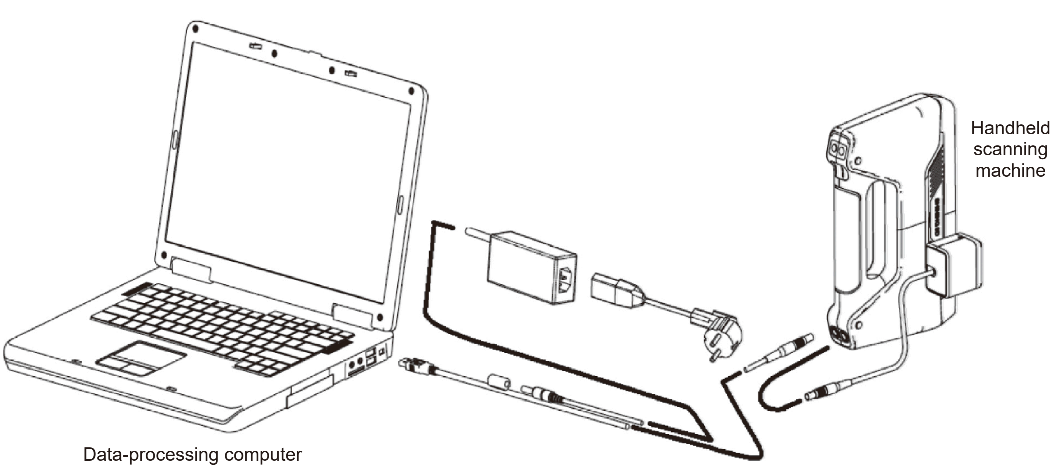

Fig. 3. 3D scanning system based on the principle of optical triangulation.

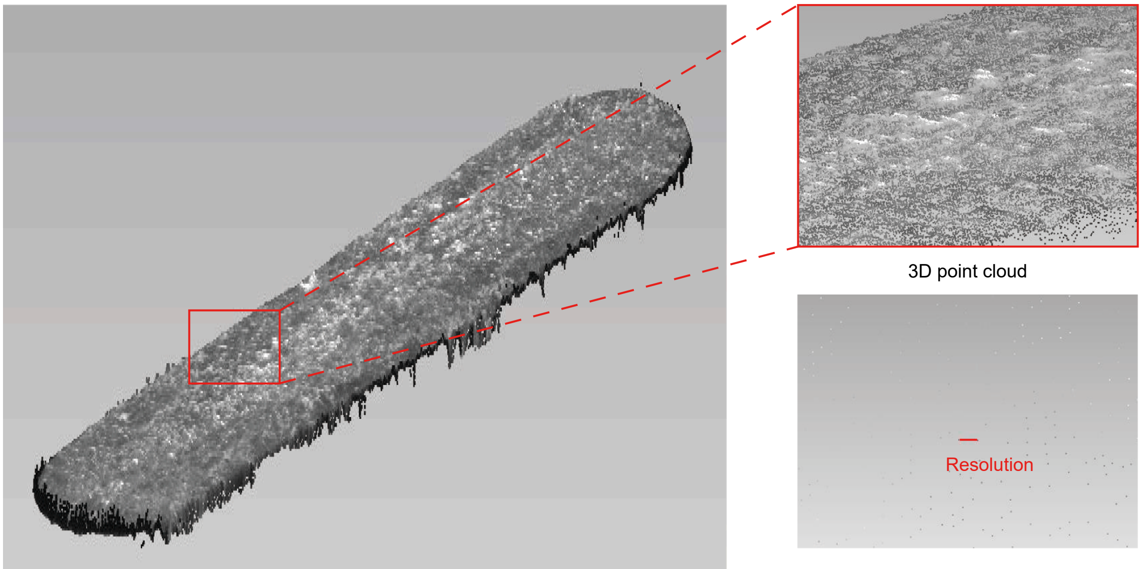

Fig. 4. 3D scanning point cloud of the fracture surface. The resolution of 3D scanning varies, the distance between points would also be different. As a result, the 3D fracture morphology obtained would also be different in terms of details.

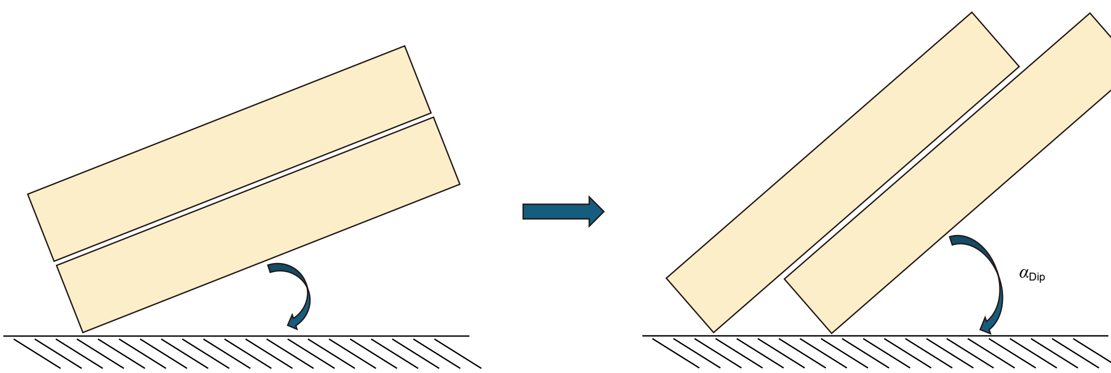

Fig. 5. The tilt test used for evaluating the JRC.

angle, °; JCS is the joint wall compressive strength, MPa; σ_n is the normal stress, MPa; n is the axial. Finally, the JRC is a dimensionless parameter. The larger the value of JRC is, the rougher the fracture surface is.

The Gaussian curvature is an intrinsic geometric property of a surface. By fitting the 3D points with the surrounding 8 points as local micro-surfaces, we can calculate the Gaussian curvature and evaluate the roughness degree of the local fracture surface quantitatively. Specifically, at each location along a fracture surface, there is a unique perpendicular direction corresponding to its surface orientation.

This directional vector defines a special plane known as the normal plane. Where this plane intersects with the fracture surface, it creates a distinctive contour called the normal section, whose degree of bending is quantitatively described by the normal curvature measurement. On typical fracture surfaces, this curvature measurement varies significantly depending on the orientation of the selected normal section. The extreme values observed in these measurements—specifically the greatest and smallest curvature magnitudes—are formally identified as principal curvatures. The calculation formula of Gaussian curvature is as follows:

$$K_{gc} = k_1 \cdot k_2 \tag{4}$$

Here, k_1 is the minimum principal curvatures and k_2 is the maximum principal curvatures. Mathematically, Gaussian curvature represents the multiplicative combination of these fundamental curvature parameters. The sign of Gaussian curvature determines the local topological class (elliptical, hyperbolic, or parabolic). The absolute value of Gaussian curvature measures the intensity of curvature. Larger magnitudes imply stronger local bending and roughness. Considering the above characteristics of Gaussian curvature, the absolute value of Gaussian curvature ($|K_{gc}|$) is adopted for the evaluation of local roughness.

3. Experimental results and analysis

3.1. Experimental results

After the wire cutting and acid etching, six acid-fracture surfaces of varying roughness would be prepared for the conductivity tests and 3D scanning. 3D scanning causes no harm to the fracture surface. During the 3D scanning process, there would be no

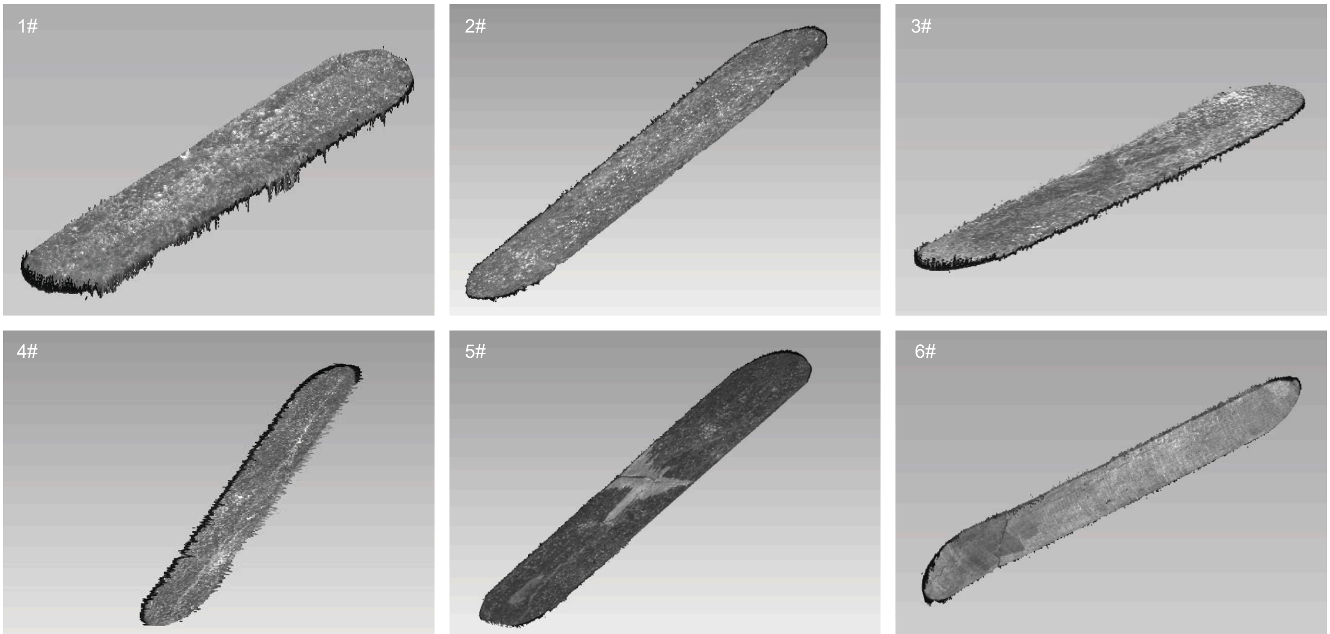

Fig. 6. Different etching times would make Samples 1# − 6# be with different levels of roughness. Before the fracture surfaces beard pressure and deform during the conductivity tests, the surfaces were scanned with 0.05 mm and other resolutions. Then the 3D cloud map would be obtained.

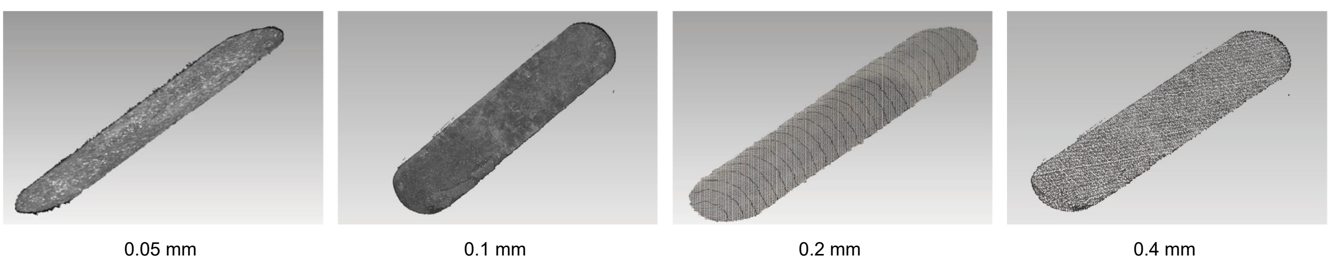

Fig. 7. Visualization of the same fracture surface scanned at four different resolutions: 0.05, 0.1, 0.2, and 0.4 mm. Each point represents a measured 3D coordinate. As the resolution decreases (from 0.05 mm to 0.4 mm), the point density becomes sparser, and the fine-scale morphological details of the surface are progressively lost.

contact and harm to the acid fracture surface. In this study, the fracture surfaces were scanned at four different resolutions: 0.05, 0.1, 0.2, and 0.4 mm. The scanning results at the resolution of 0.05 mm of Samples 1# − 6# were shown in Fig. 6.

These acid fracture surfaces were scanned at different resolutions. For the same surface, a lower scanning resolution results in a sparser point cloud. This is because the distance between the 3D points was larger. It is shown in Fig. 7.

Subsequently, we conducted tilt tests to obtain the joint roughness coefficient of each surface. During the tilting, there would inevitably be slight friction between the fracture surfaces. However, considering that in the subsequent conductivity test, the fracture surfaces would be subjected to high pressure, we can ignore the minor damage to the surfaces during this process. The JRC values of each acid fracture surfaces were shown in Table 3.

Finally, the conductivity tests were conducted. The etched rock plates were loaded into the diversion chamber and different closure pressures were set to test the conductivity. The experiment results were shown in Fig. 8.

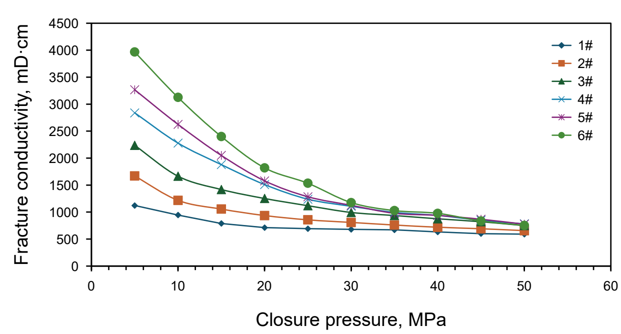

Fig. 8. The experimental results of acid fracture conductivity for Samples 1# to 6#. The results show that conductivity generally increases with acid etching time at low closure pressures (<30 MPa). However, under high closure pressures (>30 MPa), the conductivity of heavily etched samples (e.g., 5#, 6#) decreases significantly, indicating the collapse of acid-weakened asperities.

Table 3
The JRC values of acid fractures by tilt tests.

No.	Acid etching time, min	JRC
1#	0	1.09
2#	5	1.14
3#	10	2.09
4#	15	2.12
5#	20	2.14
6#	25	2.72

According to Table 3 and Fig. 8, there was a pronounced relationship between acid etching time and both fracture surface roughness and conductivity. In Sample 1#, the fracture surface was only subjected to wire-cutting and was not acid etching. The JRC of fracture surface was 1.14 and the fracture conductivity was low at any closure pressure. The main reason is that the Sample 1# was almost a flat surface due to the wire cutting. The overall roughness was relatively low, and it would be almost completely closed under the closure pressure. With the increasing of acid etching time, the JRC increased from 1.09 to 2.72 progressively. This is because that extending acid-rock interaction would enhance the roughness of the fracture surface by selectively dissolving carbonate minerals, thereby creating irregular asperities and increasing the heterogeneity of the etched morphology. Under the same closure pressure, the rougher the fracture surface was, the higher the conductivity was. This trend was particularly evident in the conductivity results of Samples 1#–6# with low closure pressure (lower than 30 MPa), but was not clear enough in the conductivity results of Samples 1#–6# with high closure pressure (larger than 30 MPa). It is demonstrated that the high conductivity resulting from long acid etching time cannot be maintained under high closure pressure. This is mainly because acid etching would lead to a reduction in the strength of the fracture surface, a higher degree of deformation under high closure pressure, and a more decline in the fracture conductivity.

3.2. *Effect of acid etching*

The absolute Gaussian curvature ($|K_{gc}|$) was used to study the detail of fracture surface and evaluate the local roughness. According to the calculation process introduced in Section 2.4, the Gaussian curvature was controlled by the scanning resolution. In this section, we conducted the Gaussian curvature calculation based on a resolution of 0.05 mm, which was the highest resolution in our study. The results of Sample 1# was shown in Fig. 9.

High-resolution scanning results can reveal more details. After calculating the absolute value of the Gaussian curvature for Sample 1#, it is even able to observe the cutting stripes caused by the wire cutting process (Fig. 9(a)). The absolute Gaussian curvature results were shown in Fig. 9(b). At a resolution of 0.05 mm, the absolute values of Gaussian curvature in Sample 1# were mainly distributed from 10^{-20} to 10^{-16}. More than 50% of the fracture surface met $|K_{gc}| < 10^{-16}$. Based on the properties of Gaussian curvature, it can be known that the larger the absolute value is, the higher the roughness at that point. The acid fracture surface obtained by wire cutting (Sample 1#) was very close to the pure plane, so the local roughness on the entire crack surface was relatively low.

Then, the following fracture surfaces were also analyzed with the same procedure. The results were shown in Fig. 10. According to the analysis principle of local roughness, red points represented micro-areas with high roughness, and blue points represented micro-areas with low roughness. With the acid etching time increased, two trends can be observed. Firstly, the randomness of the distribution of rough points also gradually increases, which can be seen from Fig. 10(a). In Sample 1#, the rough points were concentrated in the regions where the wire cutting stripes was. Compared with Sample 1#, the overall roughness of Sample 2# has increased. The roughness growth rate in wire cutting stripes was significantly higher. It is hypothesized that during the initial stage of acid etching, regions with pre-existing roughness possess a larger surface area, which promotes a more pronounced etching effect. The acid etching time continues to increase in Samples 3#, 4#, 5# and 6#, The distribution characteristics of the rough points showed an overall coordinated growth, while the local roughness distribution showed a non-coordinated feature. We speculated that this phenomenon is attributable to the randomness of fluid flow velocity and mineral distribution.

Secondly, the proportion of rough points increased with the acid etching time. The proportion of red points on the Samples 2#, 3#, 4#, 5# and 6# gradually raised, and the proportion of rough points in the Sample 6# was the highest. It can be observed from Fig. 10(b) that the main peak of the $|K_{gc}|$ distribution distinctly shifts toward higher values with the increase of acid-etching time. The log-normal distribution formula was used to describe this data distribution quantitatively:

$$f(x) = A\exp\left(-\frac{(\log_{10}x-\mu)^2}{2\sigma^2}\right). \quad (5)$$

The A, σ, and μ determine the data distribution. Following data fitting, the data distribution in Fig. 10(b) was found to correspond to the formulas with the coefficients in Table 4.

The coefficients in Table 4 quantitatively describe the evolution of the fracture surface. The μ increased from −33.024 to −15.890, which confirmed the peak shift toward higher curvature values, indicating progressively rougher surfaces with extended etching. The decreasing of σ and A verified that acid etching changed both the magnitude and spatial distribution of surface curvature. These results underscore the critical role of acid etching in tailoring fracture roughness and conductivity. By analyzing the local

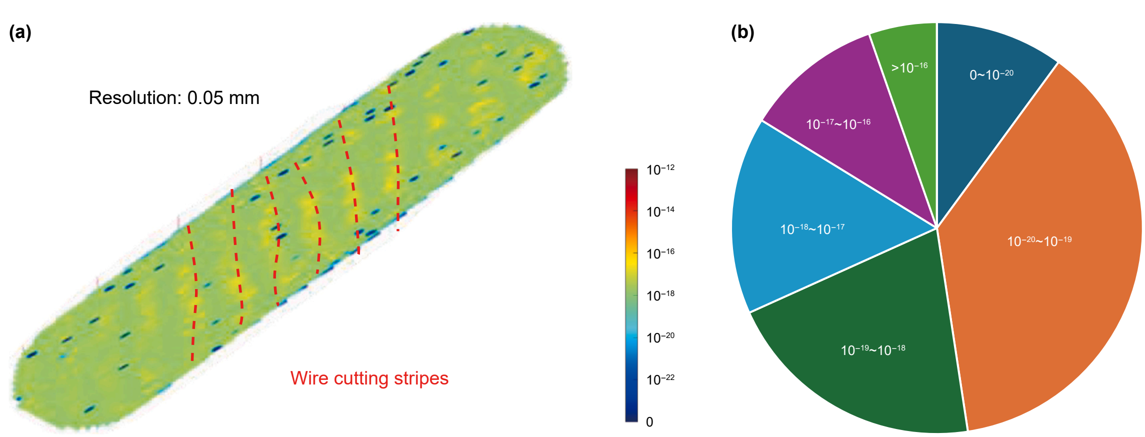

Fig. 9. Local roughness of the non-etched, wire-cut surface (Sample 1#) based on Gaussian curvature evaluation: **(a)** Cloud map of local roughness colored by the calculated $|K_{gc}|$ values. The initial surface was smooth enough to see the cutting stripes caused by the wire-cutting. **(b)** Distribution of absolute Gaussian curvature. The concentration of values at very low magnitudes (mainly distributed from 10^{-20} to 10^{-16}).

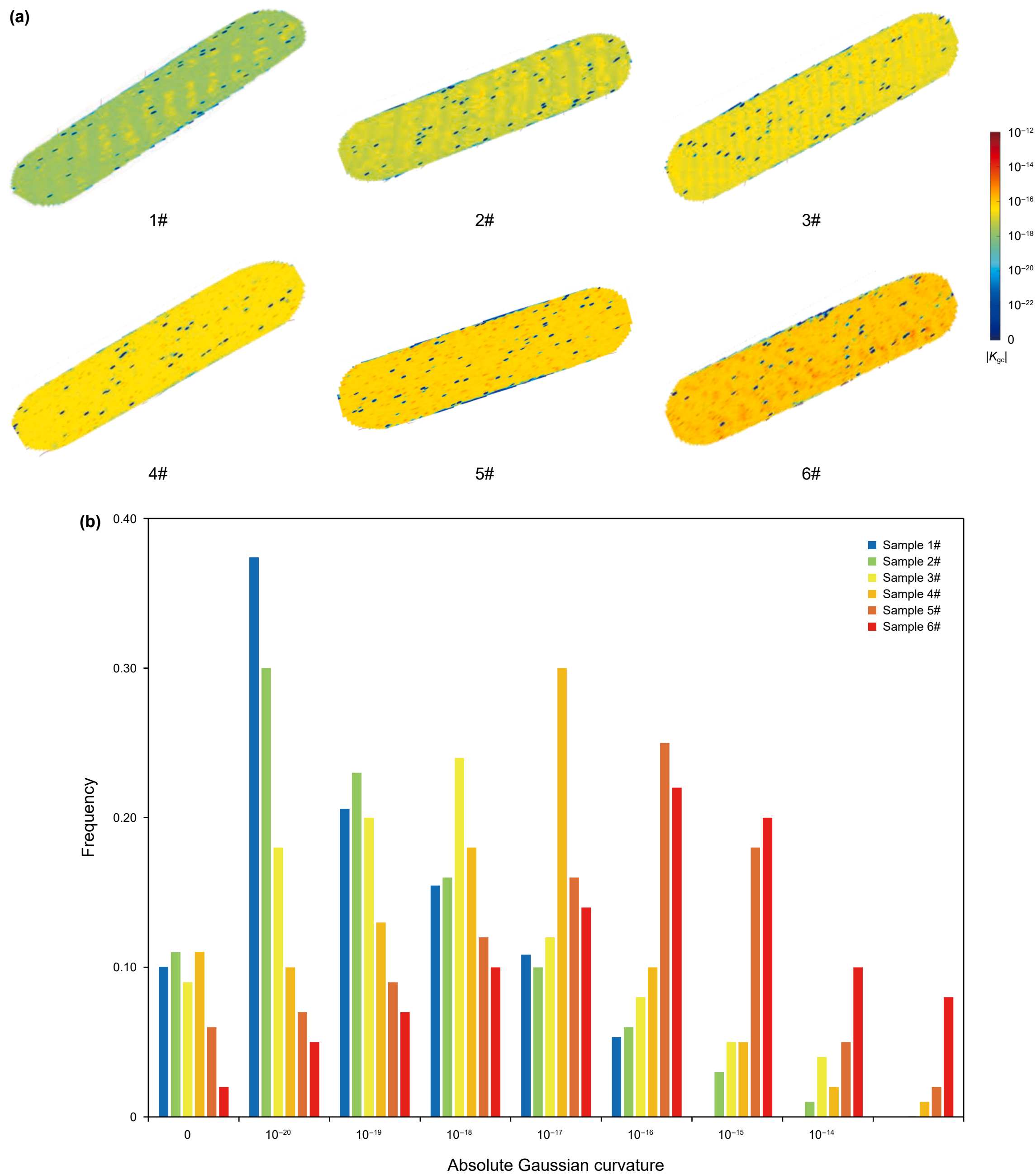

Fig. 10. Local roughness of Samples 1#–6# based on Gaussian curvature evaluation ($|K_{gc}|$) at the resolution of 0.05 mm. Red points represented micro-areas with high roughness, and blue points represented micro-areas with low roughness. **(a)** Local roughness map of Samples 1#–6#. The randomness of the distribution of rough points gradually increased with the acid etching. **(b)** Frequency distribution of absolute Gaussian curvature in Samples 1#–6#. With the acid etching time increased, the proportion of rough points would increase from Sample 1# to Sample 6#.

Table 4
The fitting coefficient in normal distribution formula.

No.	A	μ	σ
Sample 1#	4.904	−33.024	5.685
Sample 2#	0.303	−19.340	1.420
Sample 3#	0.244	−18.560	0.890
Sample 4#	0.300	−17.000	0.850
Sample 5#	0.251	−15.960	0.710
Sample 6#	0.222	−15.890	0.780

roughness based on absolute Gaussian curvature ($|K_{gc}|$), it was explained from a microscopic perspective that how acid etching causes the global roughness increasing.

3.3. Correlation analysis between roughness and conductivity

In Sections 3.1 and 3.2, global roughness and local roughness were evaluated quantitatively. It can be illustrated that acid etching would lead to increasing in both the roughness and the conductivity. Correlation coefficient was used in our research to quantitatively evaluate the correlation between roughness and conductivity. The correlation coefficient (short for COR) can quantify the strength and direction of the relationship between two variables. It ranges from −1 (perfect negative relationship) to +1 (perfect positive relationship), with 0 indicating no relationship.

$$\mathrm{COR}=\frac{\mathrm{cov}(p,q)}{\sqrt{D(p)}\sqrt{D(q)}} \tag{6}$$

Here, m, n are the two variable arrays; $\mathrm{cov}(p,q)$ is the covariance between m and n; $D(p)$, $D(q)$ are the variance of p and q, respectively.

The correlation analysis was conducted between the roughness and the fracture conductivity under different closure pressures. JRC is the single value to evaluate the global roughness of one fracture surface, which can directly applied in correlation analysis. The absolute Gaussian curvature ($|K_{gc}|$) is an array that describes the local roughness of one fracture surface, which requires us to use descriptive statistics to do correlation analysis. In this research, mean ($|K_{gc}|_{mean}$), median ($|K_{gc}|_{median}$), and variance ($|K_{gc}|_{variance}$) were chosen for analysis. Given the characteristic that the Gaussian curvature distribution spans several orders of magnitude, we also conducted further correlation analysis after taking the logarithm of descriptive statistics ($\log_{10}|K_{gc}|_{mean}$, $\log_{10}|K_{gc}|_{median}$ and, $\log_{10}|K_{gc}|_{variance}$). The correlation analysis results are shown in Fig. 11.

These seven methods (JRC, $|K_{gc}|_{mean}$, $|K_{gc}|_{median}$, $|K_{gc}|_{variance}$, $\log_{10}|K_{gc}|_{mean}$, $\log_{10}|K_{gc}|_{median}$ and $\log_{10}|K_{gc}|_{variance}$) were used to evaluating the roughness. It can be observed that roughness based on JRC evaluation has a good correlation with conductivity. $|K_{gc}|_{variance}$ and $\log_{10}|K_{gc}|_{variance}$ have little correlation with conductivity, which means variance was not a suitable method to summarize the local roughness. $|K_{gc}|_{mean}$ and $|K_{gc}|_{median}$ have positive but not good enough correlation with conductivity, which might be due to the cross-magnitude data-distribution problem. The roughness based on $\log_{10}|K_{gc}|_{median}$ has the best correlation, which means that this method has sufficient potential to be combined with Gaussian curvature for related research.

In the low closure pressure (lower than 30 MPa), JRC has the correlation coefficient over 0.92 and $\log_{10}|K_{gc}|_{median}$ has the correlation coefficient over 0.94. In the high closure pressure (larger than 30 MPa), all methods have a decreasing in correlation. This phenomenon may be due to the increased deformation under high closure pressure. To verify this assumption, we conducted 3D scanning and tilt tests after the conductivity experiments. The correlation was analyzed and the results were shown in Table 5.

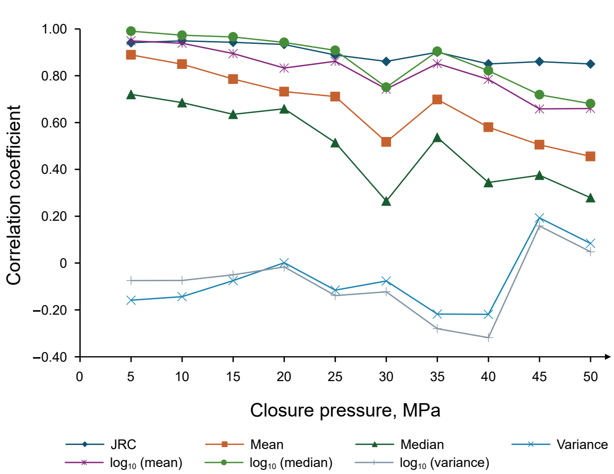

Fig. 11. Correlation coefficients between seven different roughness parameters and the measured fracture conductivity across various closure pressures. The plot identifies $\log_{10}|K_{gc}|_{median}$ was the parameter with the strongest and most consistent positive correlation with conductivity.

Table 5
The correlation analysis after the conductivity experiments.

No.	Conductivity, mD·cm	JRC	$\log_{10}|K_{gc}|_{median}$
1#	591.21	1.14	−18.90
2#	656.10	1.37	−18.52
3#	782.75	2.09	−17.38
4#	732.60	2.26	−17.87
5#	750.36	2.72	−17.90
6#	746.54	2.91	−17.81
Correlation coefficient	–	0.93	0.98

JRC and $\log_{10}|K_{gc}|_{median}$ both show a strong positive correlation with the conductivity. $\log_{10}|K_{gc}|_{median}$ has a better behavior. The above experimental analysis quantitatively analyzed the correlation between roughness and the conductivity. It is demonstrated that the reasonable method for evaluating roughness (like $\log_{10}|K_{gc}|_{median}$) can effectively correlate the conductivity of acid fractures, which is an important auxiliary tool for related research.

3.4. Estimation of the conductivity optimal correlation resolution (COCR)

In Sections 3.2 and 3.3, the relations between roughness and conductivity were studied. Significant advantages were observed in the roughness evaluation based on the Gaussian curvature from 3D scanning. It not only can evaluate the roughness from a local view (Fig. 10(a)), but also can build a strong correlation with the fracture conductivity from a global view (Fig. 11 and Table 5).

The resolution of 3D scanning has a significant effect on the evaluation, which can be seen in Fig. 12. As the resolution changed from 0.05 mm (high resolution) to 0.4 mm (low resolution), the distribution of $|K_{gc}|$ gradually became concentrated and the magnitude increased with the resolution. This indicates that lower resolutions lead to the loss of fine surface detail, resulting in an apparent smoothing effect that manifests as both higher calculated Gaussian curvature magnitudes and a narrower spread of values, as subtle variations are averaged out or omitted.

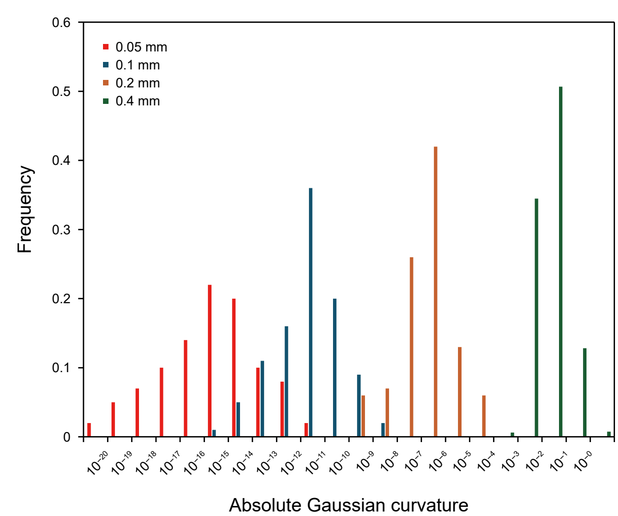

Fig. 12. The impact of 3D scanning resolution on the calculated distribution of absolute Gaussian curvature ($|K_{gc}|$) for Sample 6#. As the scanning resolution coarsens (from 0.05 mm to 0.4 mm), the distribution of $|K_{gc}|$ becomes narrower and shifts towards higher magnitudes. This indicates that lower resolutions fail to capture fine-scale surface details, resulting in an oversmoothed digital model that overestimates the average curvature and underestimates the true morphological complexity.

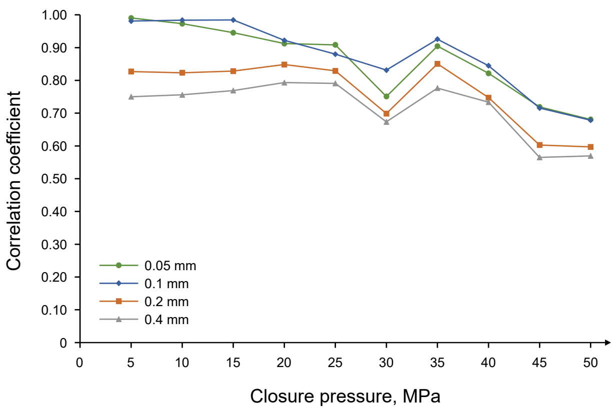

Fig. 13. Correlation coefficient between the ($\log_{10}|K_{gc}|_{median}$) roughness parameter and fracture conductivity, plotted against closure pressure for four different scanning resolutions. The correlation is strongest and most stable across low closure pressures when using a resolution of 0.1 mm. Both higher (0.05 mm) and lower (0.2 mm, 0.4 mm) resolutions yield weaker correlations. This identifies 0.1 mm as the COCR, providing the most representative digital description of the fracture surface for conductivity prediction.

Using insufficient resolution may lead to a systematic misunderstanding of the surface complexity, which potentially leading to erroneous conclusions about the characteristics of the scanned surface. Considering that the digital research on the acid fracture surface is mainly aimed at providing assistance for the analysis of conductivity, the correlation analysis was conducted under different resolution. $\log_{10}|K_{gc}|_{median}$ was chosen as the evaluation method. The results were shown in Fig. 13.

Under the same roughness analysis procedure, the correlation would change with the resolution. When the closure pressure was over 30 MPa, the correlation coefficients all lost the regularity. This phenomenon was also observed in Section 3.3. Thus, we focused more on the correlation data at low closure pressure. In the resolution of 0.4 mm and 0.2 mm, the correlations were positive but not strong enough. In the resolution of 0.1 mm and 0.05 mm, the correlations were strongly high. In the low closure pressure conditions, the correlation behavior in the resolution of 0.1 mm exceeds the performance achieved at the resolution of 0.05 mm. This means that once the resolution reaches the level of 0.1 mm, further increasing the resolution would not bring any benefits to the digital analysis of fracture conductivity. There is even a possibility that, at extremely high resolutions, over-detailed 3D-scanning descriptions of acid fractures may cause interference (similar to over-fitting phenomenon) in the analysis of the fracture conductivity.

Thus, the resolution of 0.1 mm was found and defined as the COCR in acid fracture analysis. The roughness evaluated at that resolution has the best correlation with the acid fracture conductivity.

4. Discussion

The experimental results showed that acid etching would increase fracture roughness and conductivity, yet this effect diminishes under high closure pressures. This behavior can be attributed to the chemo-mechanical weakening of the fracture surface. Acid dissolution preferentially attacks carbonate minerals, creating localized asperities and increasing surface heterogeneity. However, the same process reduces the mechanical strength of the rock matrix, leading to greater plastic deformation and asperity collapse under high stress. This dual effect, enhanced roughness versus reduced strength, explains why conductivity gains are more pronounced at lower closure pressures. Gaussian curvature identifies micro-scale features that act as preferential flow channels or mechanical anchors, thereby offering a more mechanistic link between morphology and conductivity. The Gaussian curvature-based roughness can capture localized curvature variations that directly influence fluid flow paths.

Fracture conductivity tests in laboratory are inherently destructive, often leading to significant breaking on the fracture surface under high closure pressure. This destruction brings a major challenge for repeated experiments or further morphological analysis on the same sample, thereby limiting the reproducibility of experiments and depth of investigation. Digital rock analysis (including 3D scanning and 3D printing) has become an emerging trend in rock mechanics research, with 3D scanning and serving as a quintessential enabling technology in this domain. The key to this digital workflow lies in acquiring a high-fidelity digital model. Resolution constitutes a critical parameter in 3D scanning, fundamentally determining whether the acquired data possesses sufficient fidelity to support subsequent analyses. Existing researchers often conduct the 3D scanning with the highest available resolution. This strategy seems to be intuitively reasonable. However, different researchers have different scanning technologies supports in different periods or institutions, which means the highest available resolution is a standard that varies from person to person. What's more, increasing resolution would lead to substantial costs and overwhelming data requiring processing. Our experimental evidence demonstrates that heightened resolution does not invariably yield stronger correlations between the roughness and conductivity (Section 3.4). Therefore, the concept of COCR is proposed not only as a cost-saving measure, but also as a scientifically justified criterion to ensure that the digital representation of fracture surfaces aligns optimally with their hydraulic performance.

For proppant-filled fractures, the conductivity is primarily governed by the arrangement, embedment, and crushing behavior of the proppant pack, rather than the etched morphology of the rock surface. Directly applying the COCR of 0.1 mm from this study to correlate with conductivity may no longer be optimal. For self-supporting fractures in shale formations, the mechanism is closer to that of acid-etched fractures, as both rely on the rough fracture morphology to resist closure stress. Therefore, the proposed method holds significant potential for applicability.

Consequently, we posit that selecting an appropriate resolution is the optimal strategy for 3D scanning applications. The identification of COCR provides a practical guideline for digital rock analysis. In practice, this resolution strikes a balance between data fidelity and computational efficiency, enabling reliable digital results of fracture surfaces without excessive data overhead. The COCR represents the critical threshold that mainly impact fluid flow in acid fracture surface. It provides the essential resolution standard for accurately characterizing the surface topology in fracture conductivity research, providing the benchmark for future studies on more complex, heterogeneous systems.

5. Conclusions

This study conducted 3D scanning, fracture conductivity tests, and roughness evaluations on acid fractures. The experimental results were then combined and analyzed. The resolution selection criterion was established for 3D scanning to maximize the roughness and conductivity correlation in acid fracture. The final conclusions are as follows.

(1) It is quantitatively demonstrated that acid etching enhances fracture roughness Extending acid etching time would

progressively increase both global roughness and local heterogeneity, which can be obtained through the analysis of the surface roughness. It would lead to flow pathways under closing pressure by creating asperities that resist full closure.

(2) The roughness evaluation based on Gaussian curvature from 3D scanning showed great advantages. It not only can evaluate the roughness from a local view, but also can build a global evaluation method ($\log_{10}|K_{gc}|_{median}$), which has a strong correlation with the fracture conductivity. Compared with experimental methods for roughness evaluating, this method has the advantage of being no-damage to the fracture surface and having a high degree of digitization.

(3) The roughness showed scale-dependent correlations with conductivity. In acid fracture research, scanning at the resolution of 0.1 mm would maximize the roughness-conductivity correlation. This resolution can be defined as COCR. Higher resolutions (0.05 mm) or lower resolutions (0.2 mm, 0.4 mm) would reduce correlation because of over fitting or morphological details losing. The COCR provides a cost-effective standard for digital acid fracture analysis.

CRediT authorship contribution statement

Yi-Fan Dai: Formal analysis, Data curation, Conceptualization. **Zhen-Yu Wang:** Investigation, Formal analysis. **Lin-Jun Zou:** Investigation, Formal analysis. **Ming-Fang He:** Formal analysis. **Shi-Hui Gao:** Formal analysis. **Bing Hou:** Software, Investigation.

Declaration of competing interest

The authors declare that they have no known competing financial interests or personal relationships that could have appeared to influence the work reported in this paper.

Acknowledgements

The authors are grateful for the support from Science and Technology Program of Xinjiang Uyghur Autonomous Region (No. 2024B1014) and National Science and Technology Major Project of China (No. 2024ZD14047001) and National Science and Technology Major Project (No. 2025ZD1402500) and Xinjiang Key Laboratory of Carbon Efficient Utilization and Storage (No. XJCCUS202505).

References

Al-Anazi, H., Nasr-El-Din, H., Mohamed, S., 1998. Stimulation of tight carbonate reservoirs using acid-in-diesel emulsions: Field application. In: SPE International Conference and Exhibition on Formation Damage Control, SPE-39418-MS. https://doi.org/10.2118/39418-MS.

Aljawad, M.S., Schwalbert, M.P., Zhu, D., et al., 2020. Improving acid fracture design in dolomite formations utilizing a fully integrated acid fracture model. J. Petrol. Sci. Eng. 184, 106481. https://doi.org/10.1016/j.petrol.2019.106481.

Andrews, J.W., 2020. Hydrogen production and carbon sequestration by steam methane reforming and fracking with carbon dioxide. Int. J. Hydrogen Energy 45, 9279–9284. https://doi.org/10.1016/j.ijhydene.2020.01.231.

Arakawa, K., Takahashi, K., 1991. Relationships between fracture parameters and fracture surface roughness of brittle polymers. Int. J. Fract. 48, 103–114. https://doi.org/10.1007/BF00018393.

Asadollahpour, E., Baghbanan, A., Hashemolhosseini, H., et al., 2018. The etching and hydraulic conductivity of acidized rough fractures. J. Petrol. Sci. Eng. 166, 704–717. https://doi.org/10.1016/j.petrol.2018.03.074.

Bale, A., Smith, M.B., Klein, H.H., 2010. Stimulation of carbonates combining acid fracturing with proppant (CAPF): A revolutionary approach for enhancement of sustained fracture conductivity and effective fracture half-length. In: SPE Annual Technical Conference and Exhibition,. https://doi.org/10.2118/134307-MS. SPE-134307.

Brasington, J., Vericat, D., Rychkov, I., 2012. Modeling river bed morphology, roughness, and surface sedimentology using high resolution terrestrial laser scanning. Water Resour. Res. 48, W11519. https://doi.org/10.1029/2012WR012223.

Chen, C., Martysevich, V., Oconnell, P., et al., 2015. Temporal evolution of the geometrical and transport properties of a fracture/proppant system under increasing effective stress. SPE J. 20, 527–535. https://doi.org/10.2118/171561-PA.

Dai, Y., Hou, B., Zhou, C., et al., 2021. Interaction law between natural fractures vugs and acid-etched fracture during steering acid fracturing in carbonate reservoirs. Geofluids 2021, 1–16. https://doi.org/10.1155/2021/5581179.

Feng, W., Yang, C., Zhou, F., 2021. Experimental study on surface morphology and relevant plugging behavior within acid-etched and unetched fractures. J. Nat. Gas Sci. Eng. 88, 103847. https://doi.org/10.1016/j.jngse.2021.103847.

Gou, B., Li, X., Guo, J., et al., 2023. Effect of acid type on acid-etched fracture surface morphology and conductivity along the fracture. Energy Fuel. 37, 3709–3722. https://doi.org/10.1021/acs.energyfuels.2c04076.

Guo, J., Wang, J., Liu, Y., et al., 2017. Analytical analysis of fracture conductivity for sparse distribution of proppant packs. J. Geophys. Eng. 14, 599–610. https://doi.org/10.1088/1742-2140/aa63b1.

Hou, B., Dai, Y., Zhou, C., et al., 2021. Mechanism study on steering acid fracture initiation and propagation under different engineering geological conditions. Geomech. Geophys. Geo-Energy Geo-Resour. 7, 73. https://doi.org/10.1007/s40948-021-00271-x.

Hou, T., Zhang, S., Ma, X., et al., 2017. Experimental and theoretical study of fracture conductivity with heterogeneous proppant placement. J. Nat. Gas Sci. Eng. 37, 449–461. https://doi.org/10.1016/j.jngse.2016.11.054.

Kerckhofs, G., Pyka, G., Moesen, M., et al., 2013. High-resolution microfocus X-ray computed tomography for 3D surface roughness measurements of additive manufactured porous materials. Adv. Eng. Mater. 15, 153–158. https://doi.org/10.1002/adem.201200156.

Lai, J., Guo, J., Ma, Y., et al., 2022. Effect of acid–rock reaction on the microstructure and mechanical property of tight limestone. Rock Mech. Rock Eng. 55, 1–15. https://doi.org/10.1007/s00603-021-02650-5.

Lange, D.A., Jennings, H.M., Shah, S.P., 1993. Relationship between fracture surface roughness and fracture behavior of cement paste and mortar. J. Am. Ceram. Soc. 76, 589–597. https://doi.org/10.1111/j.1151-2916.1993.tb03646.x.

Li, B., Wang, J., Liu, R., et al., 2021. Nonlinear fluid flow through three-dimensional rough fracture networks: insights from 3D-printing, CT-scanning, and high-resolution numerical simulations. J. Rock Mech. Geotech. Eng. 13, 1020–1032. https://doi.org/10.1016/j.jrmge.2021.04.005.

Li, Y., Jiang, X., Tang, J., et al., 2024. Simulation study of acid fracturing initiation with consideration of rock mechanics parameter variations. Rock Mech. Rock Eng. 57, 5743–5761. https://doi.org/10.1007/s00603-024-03844-3.

Li, Y., Zhang, Y., 2015. Quantitative estimation of joint roughness coefficient using statistical parameters. Int. J. Rock Mech. Min. Sci. 77, 27–35. https://doi.org/10.1016/j.ijrmms.2015.03.016.

Li, Z., Zhao, Q., Teng, Y., et al., 2022. Experimental investigation of non-monotonic fracture conductivity evolution in energy georeservoirs. J. Petrol. Sci. Eng. 211, 110103. https://doi.org/10.1016/j.petrol.2022.110103.

Liu, Y., Wu, L., Guo, J., et al., 2024. Model for fracture conductivity considering particle size redistribution caused by proppant crushing. Geoenergy Sci. Eng. 240, 213081. https://doi.org/10.1016/j.geoen.2024.213081.

Malagon, C., Pournik, M., Hill, A.D., 2008. The texture of acidized fracture surfaces: implications for acid fracture conductivity. SPE Prod. Oper. 23, 343–352. https://doi.org/10.2118/107505-PA.

Mendez-Vilas, A., Bruque, J., González-Martín, M., 2007. Sensitivity of surface roughness parameters to changes in the density of scanning points in multi-scale AFM studies: Application to a biomaterial surface. Ultramicroscopy 107, 617–625. https://doi.org/10.1016/j.ultramic.2006.12.002.

Prajapati, D.K., Tiwari, M., 2017. Topography analysis of random anisotropic gaussian rough surfaces. J. Tribol. 139, 041402. https://doi.org/10.1115/1.4035650.

Qi, C., Liu, Y., Dong, F., et al., 2020. Study on heterogeneity of pore throats at different scales and its influence on seepage capacity in different types of tight carbonate reservoirs. Geofluids 2020, 6657660. https://doi.org/10.1155/2020/6657660.

Rashid, F., Glover, P., Lorinczi, P., et al., 2015. Porosity and permeability of tight carbonate reservoir rocks in the north of Iraq. J. Petrol. Sci. Eng. 133, 147–161. https://doi.org/10.1016/j.petrol.2015.05.009.

Sun, Z., Shi, J., Wu, K., et al., 2019. A prediction model for desorption area propagation of coalbed methane wells with hydraulic fracturing. J. Petrol. Sci. Eng. 175, 286–293. https://doi.org/10.1016/j.petrol.2018.12.047.

Tatone, B.S., Grasselli, G., 2013. An investigation of discontinuity roughness scale dependency using high-resolution surface measurements. Rock Mech. Rock Eng. 46, 657–681. https://doi.org/10.1007/s00603-012-0296-2.

Tse, R., Cruden, D., 1979. Estimating joint roughness coefficients. Int. J. Rock Mech. Min. Sci. Geomech. Abstracts 16, 303–307. https://doi.org/10.1016/0148-9062(79)91240-8.

Wang, Y., Fan, Y., Zhou, C., et al., 2021. Research and application of segmented acid fracturing by temporary plugging in ultradeep carbonate reservoirs. ACS Omega 6, 28620–28629. https://doi.org/10.1021/acsomega.1c03370.

Wang, Y., Zhou, C., Yi, X., et al., 2020. Technology and application of segmented temporary plugging acid fracturing in highly deviated wells in ultradeep

carbonate reservoirs in southwest China. ACS Omega 5, 25009–25015. https://doi.org/10.1021/acsomega.0c01008.
Wei, J., Zhou, X., Fu, X., et al., 2021. Experimental investigation of long-term fracture conductivity filled with quartz sand: Mixing proppants and closing pressure. Int. J. Hydrogen Energy 46, 32394–32402. https://doi.org/10.1016/j.ijhydene.2021.07.083.
Williams, B., Nierode, D., 1972. Design of acid fracturing treatments. J. Petrol. Technol. 24, 849–859. https://doi.org/10.2118/3720-PA.
Wu, L., Liu, Y., Guo, J., et al., 2025. CFD-DEM simulation of composite plugging using novel sheet fibers in rough fractures. Energy 319, 134895. https://doi.org/10.1016/j.energy.2025.134895.
Xue, Y., Teng, T., Dang, F., et al., 2020. Productivity analysis of fractured wells in reservoir of hydrogen and carbon based on dual-porosity medium model. Int. J. Hydrogen Energy 45, 20240–20249. https://doi.org/10.1016/j.ijhydene.2019.11.146.
Yang, Y., Wen, Q., 2017. Numerical simulation of gas-liquid two-phase flow in channel fracture pack. J. Nat. Gas Sci. Eng. 43, 33–47. https://doi.org/10.1016/j.jngse.2017.03.024.
Zhang, L., Zhou, F., Mou, J., et al., 2018. A new method to improve long-term fracture conductivity in acid fracturing under high closure stress. J. Petrol. Sci. Eng. 171, 760–770. https://doi.org/10.1016/j.petrol.2018.07.073.
Zhong, Y., Kuru, E., Zhang, H., et al., 2019. Effect of fracturing fluid/shale rock interaction on the rock physical and mechanical properties, the proppant embedment depth and the fracture conductivity. Rock Mech. Rock Eng. 52, 1011–1022. https://doi.org/10.1007/s00603-018-1658-z.
Zhou, B., Jin, Y., Xiong, W., et al., 2021. Investigation on surface strength of acid fracture from scratch test. J. Petrol. Sci. Eng. 206, 109017. https://doi.org/10.1016/j.petrol.2021.109017.
Zhou, H., Wu, X., Song, Z., et al., 2022. A review on mechanism and adaptive materials of temporary plugging agent for chemical diverting fracturing. J. Petrol. Sci. Eng. 212, 110256. https://doi.org/10.1016/j.petrol.2022.110256.
Zimmerman, R.W., Bodvarsson, G.S., 1996. Hydraulic conductivity of rock fractures. Transport Porous Media 23, 1–30. https://doi.org/10.1007/BF00145263.